Wear 518–519 (2023) 204635

Contents lists available at ScienceDirect

Wear

journal homepage: www.elsevier.com/locate/wear

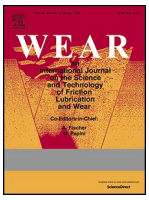

Friction, wear, and airborne particle emissions from rail-wheel contact with laser cladded overlays - A pin-disc tribometer simulation

Nashit Ali [a,*], Ulf Olofsson [b], Senad Dizdar [c]

[a] University of Bologna, Department of Industrial Engineering, Research Laboratory, Via Umberto Terracini 24, 40131, Bologna, Italy
[b] KTH Royal Institute of Technology System and Component Design, SE 100 44, Stockholm, Sweden
[c] Halmstad University, Box 823, S-301 18, Halmstad, Sweden

ARTICLE INFO

Keywords:
Friction
Wear
Airborne particle emission
Rail-wheel contact
Laser cladding
Solid lubricant

ABSTRACT

The present study uses a pin-on-disc tribometer to evaluate friction, wear, and airborne particle emissions for a rail-wheel contact. Test pins from UIC60 900A rail carbon steels were in contact with three types of test discs surfaces: R7 wheel carbon steel, laser cladding overlayed martensitic stainless steel, and laser cladding overlayed Ni-based-8% MnS self-lubricating alloy. Test results show about halving of the coefficient of friction, 0.42 to 0.22, and one ten-power lower specific pin and disc wear of discs with self-lubricating overlay compared to standard railway carbon steel contacts. Using stainless-steel overlayed discs also resulted in one ten-power lower specific disc wear, but pin wear is unchanged. Particle emission for the tests with discs with self-lubricating overlay is constant at almost 200 particles/cm^3 while running in the distance is needed for the other tests. Almost all generated airborne wear particles were in the sub-100 nm range. The use of laser-cladded (LC) overlay reduced the number of airborne wear particles in the sub-100 nm range by more than a factor of 10.

1. Introduction

Population growth in urban areas has boosted the enthusiasm for constructing Urban Rail Transit Systems (URTs), considered "green transportation" worldwide. There are numerous advantages to URTs, including their large capacity, high efficiency, and little floor space requirements, making them a viable alternative to road traffic congestion and environmental pollution [1]. Subways are one of the means of URTs that begin (in London) in the late 19th century and nowadays, almost 125 years later, carry more passengers than any other city transport mode worldwide. Thus, it has become an everyday part of millions of commuters that spend a portion of their time on subway trains. One of the major drawbacks of any underground transport system is that it operates in a confined space that may permit the accumulation of unhealthy concentrations of airborne contaminants [2]. Therefore, maintaining air quality in subway environments is essential [3].

At rail subway platforms, extremely small (nanometric to a few microns in size) particle generations occur at the brake-wheel and wheel-rail interfaces that are highly ferruginous [4]. Such wear particles have the potential to be dispersed by air since they will have a terminal velocity slow enough to become airborne [5]. The metalliferous character of these particles has the potential to cause DNA damage [6].

The loading conditions and contact geometries in wheel-rail contact mechanics vary as the train progresses down the track. The wheel-rail contact (typically 1 cm^2) mainly occurs at the wheel tread-rail head in tangent tracks at large curvature radii and wheel flange-rail gauge corner in curves with small curvature radii, see Fig. 1, with two typical wear appearances. Both rail head and wheel are made of pearlitic steel and therefore undergo adhesive wear under the influence of sliding and rolling [7]. Lewis and Olofsson [8] identified the wear regimes and transitions by developing wear maps in terms of slip and contact pressure and showed that mild to severe wear results from contact conditions most likely to occur in the wheel tread/railhead contact, and severe to catastrophic wear, in the wheel flange/rail gauge corner, contact. Liu et al. [9] studied the influence of sliding velocity on particle generation in dry sliding wheel-rail contact in the lab environment and showed that the particle number concentration level remarkably increases with an increased sliding velocity. Thus, wheel-rail sliding contact's severe to catastrophic wear contributes to high particulate matter emission.

Sund et al. [10] experimentally simulated by using pin-on-disc testing that the change in wear mechanism and wear rate in a wheel-rail contact can be detected by measuring the number of airborne particles. Laser cladding, an overlay welding technology, has been evaluated with successful results in improving the wear resistance of

* Corresponding author.
E-mail address: nashit.ali93@gmail.com (N. Ali).

https://doi.org/10.1016/j.wear.2023.204635
Received 11 September 2022; Received in revised form 30 November 2022; Accepted 22 January 2023
Available online 24 January 2023

rail-wheel contact in many studies [11–15]. Fig. 2(a) shows a schematic of laser cladding, while Fig. 2(b) illustrates typical rail/wheel regions for profile restoration and friction-wear reduction by weld overlay technology such as laser cladding. In the laser cladding process, an overlay layer is welded onto the substrate surface by using a laser beam with a very high-power concentration compared to more conventional overlay welding technologies such as an electrode, MIG and TIG, see Fig. 2(a). That high laser beam power concentration allows the deposition of overlays with metallurgical bonding to the substrate but with only between 2 and 5% dilution and reduced thermal deformation of the substrate workpiece [16]. In common, laser cladding has an overlaying rate of 10–50 cm^2/min with overlay thickness in a range from 50 μm to 2 mm, whereas a much recent development by Fraunhofer termed Extreme High-Speed Laser cladding (German acronym: EHLA) is capable of producing much thinner overlays of about 25–250 μm with a surface rate that can reach 500 cm^2/min [17]. Laser cladding is commonly performed in laser cladding workshops under controlled environment conditions, necessary precautions and safety measures such as compulsory eye-protection glasses. For open-air applications such as railway and tram rails, in-situ laser cladding with mobile laser systems, e.g. Laserline LDF Series - Mobile High Power Diode Laser [18], has been practised with promising results [19]. The laser cladding operators use fences – a well-known welders' measure to protect the melt pool from wind and achieve eye-protection of people and animals from fences from the welding arc light/laser light.

The wheel-rail contact is an open system, similar to the brake disc system of automobiles. Olofsson et al. [20] and Lyu et al. [21] showed that laser cladding can be applied successfully to repair worn-out brake rotors. Dizdar et al. [22] investigated dry sliding conditions in a pin-on-disc tribometer equipped with particle analysis equipment that, wear and particle emission of LC (with a powder mix of Ni-self fluxing alloy + 60% spheroidized fused tungsten carbide) Grey Cast Iron (GCI) brake disc was reduced as compared with traditional GCI brake disc. Olofsson et al. [20] simulated in a pin-on-disc tribometer that the wear and particle emissions of the disc brake against the same pad material were higher when LC with martensitic stainless steel powder to one compared to the original cast iron. Hence, the laser cladding process must also be tuned by selecting a suitable metal powder consumable that fulfils the specified requirements. The effect of a friction modifier can be defined as the ability to reduce friction in a sliding contact of metallic members [23] and can be applied to wheel-rail contact to generate the required coefficient of friction [24]. Abbasi et al. [25] performed a pin-on-disc study of the effects of railway friction modifiers on airborne wear particles from wheel-rail contacts. The number of particles reduced with the grease, but the number of ultrafine particles increased with the water-based friction modifier, mainly due to water vaporisation.

Therefore, in the authors' view, rail-wheel contact has not been studied so far in the context of laser cladding to reduce particle emissions. The present study aims to evaluate the wear and airborne particle emissions for rail-wheel contact simulated in a lab environment. Traditional UIC60 900A rail and R7 wheel materials were compared with two LC rail material discs.

2. Experimental methodology

2.1. Test Set-up.

Olofsson et al. [26]. Previously used the test set-up to study the airborne wear particles generated from a sliding contact. Since both rolling and sliding occur in wheel-rail contacts [27], therefore, the most common test to simulate this is the "twin-disk" machine [28]. However, in terms of the potential to cause wear, the motion tangential to the surface (sliding) is more severe than the motion perpendicular to the surface (rolling) [27]. Since high sliding velocities were used in this experiment, which required a complicated redesign, pure sliding was simulated on the pin-on-disk tribometer, as presented previously by Liu et al. [9]. However, in the present experiment, only one particle-measurement device was used to sample and collect particles.

Fig. 3 illustrates the schematic of the test set-up. The tests were performed using a pin-on-disc tribometer enclosed in a controlled climate chamber. Fan (B) supplies air to box (G) from room (A). Filter (D) ensures the filtration of air before entering through inlet (F) via flexible tube (E). The airflow inside the chamber is controlled at 0.42 m/s via the flow measurement system (C). The air inside box (N) is well-mixed due to the complex volume of the pin-on-disc machine (H). The outlet (J) is connected to the particle measuring instrument that collects the particles from the contact between pin (I) and rotating disc (M).

The tangential force is measured using an HBM® Z6FC3/20 kg load cell (non-linearity of 0.1% of the full-scale output). The coefficient of friction is then determined by dividing this measurement by the applied load.

The mass loss for specimens was measured before and after the test to the nearest 0.1 mg. SARTORIUS® ME614S and METTLER TOLEDO XP2003S were used for this measurement for pin and disc specimens, respectively. Specific wear rate k could then be determined by using Eq. (1) [22].

$$k = \frac{\Delta m}{\rho \cdot \Delta s \cdot F_N} \cdots \quad \text{Equation 1}$$

where Δm is the mass loss of the specimen, ρ *is the* specimen's density (7.58 g/cm^3), Δs is the total sliding distance, and F_N is the normal load applied to the pin.

2.1. *Particle counter instrument*

The electrical low-pressure impactor (ELPI+) developed by Dekati Ltd, Finland, was used to measure particle concentration. The operating

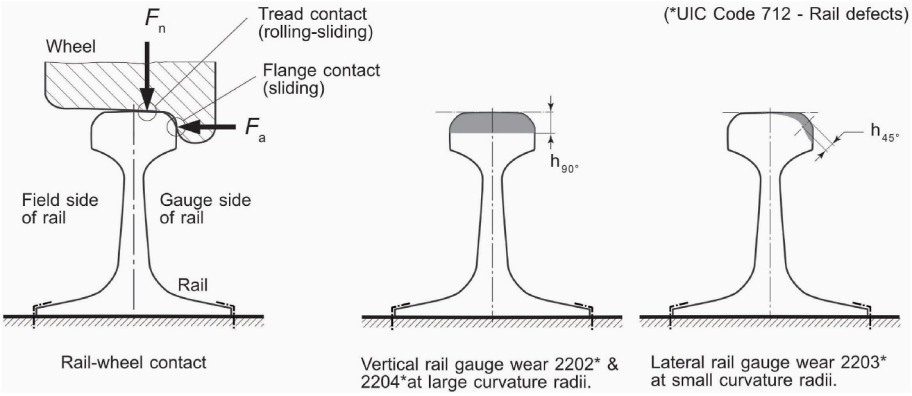

Fig. 1. Rail-wheel contact with the illustration of two typical wear damages by following UIC (International Union of Railways) rail defect codes.

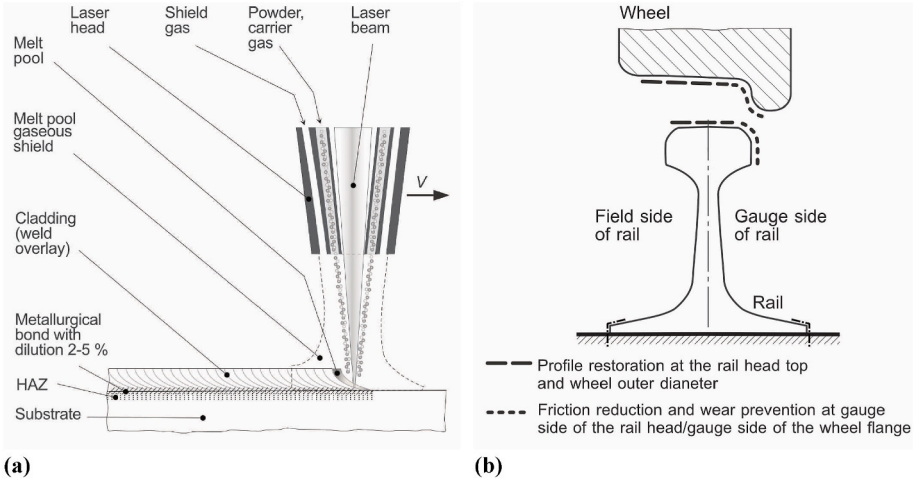

Fig. 2. Laser cladding schematic **(a)** and typical rail/wheel regions for profile restoration and friction and wear reduction by weld overlay technology such as laser cladding **(b)**.

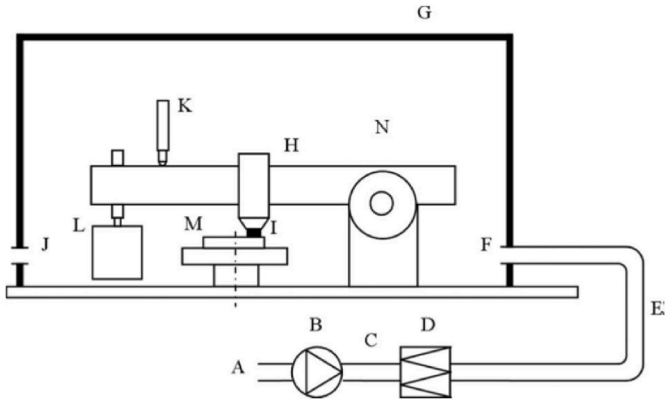

Fig. 3. Schematic of the test equipment. (A) Room air; (B) fan; (C) flow rate measurement point; (D) filter; (E) flexible tube; (F) inlet for clean air, measurement point; (G) closed box (chamber); (H) pin-on-disc machine; (N) air inside the box, well mixed; (J) air outlet, measurement points; (L) dead weight; (M) rotating disc sample; and (I) pin sample [26].

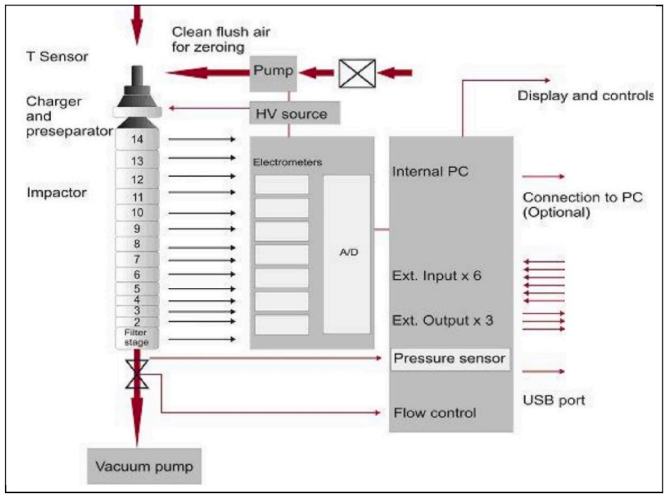

Fig. 4. Operating principle of the ELPI+ [29].

principle of ELPI+ is that the particles are charged upon passing through a unipolar corona charger (to a known positive charge level) which are then classified in a cascade impactor into 14 size classes depending on their aerodynamic size. The electrometers detect the charge carried by these particles as these particles get collected in the impactor stages. The classification of particles is based on their respective inertia, with larger particles getting collected in the upper impactor stage and smaller particles in the lower stages. ELPI + measures the particle size distribution and concentration in the particle size range of 6 nm–10 μm [29]. The particles were collected on greased aluminium filters during these 14 impactor stages. The operating principle of ELPI+ (uncertainty of less than 10% of the full-scale output) is shown in Fig. 4. The sensitivity of the ELPI + instruments is in the order of 100 no/cm^3 in the sub-100 nm particle range.

2.2. Test specimen

The pins and discs were cut from the commercial used UIC60 900A rail and R7 wheel material, respectively. Mushroom-type (round-headed) pins and cylindrical plates were manufactured as pins and discs, respectively. The sketch of both the pin and disc is given in Fig. 5. Note that the contact radius of the pins was 50 mm.

2.3. Test procedure

Except for LC discs, the specimens were cleaned by an ultrasonic bath (BRANSONIC ENA-9408) in isopropanol for 15 min just before the test run. The LC discs were carefully cleaned with wipes dipped in isopropanol. Since the LC discs had porosity on the clad, therefore, to avoid contamination, they were not put in the ultrasonic bath. A force of 60 N was applied to ensure a contact pressure of 0.3 GPa to simulate the contact pressure of the train. The force value was calculated using the Hertzian contact theory [30]. The sliding velocity (1.2 m/s) represents the extreme contact situation of the sliding wheel-rail contact corresponding to braking in sharp curves. Table 1 lists the disc and pin material properties.

Four tests were run for each of the following pin/disc combinations except for Case-1, which was repeated three times.

- Case-1 – UIC60 900A rail pin against R7 wheel disc.
- Case-2 – UIC60 900A rail pin against R7 wheel disc LC with Ni-based powder alloy containing 8% manganese sulphide (MnS).
- Case-3 – UIC60 900A rail pin against R7 wheel disc LC with 316L stainless steel.

Before starting the test, the particle concentration was tested at the

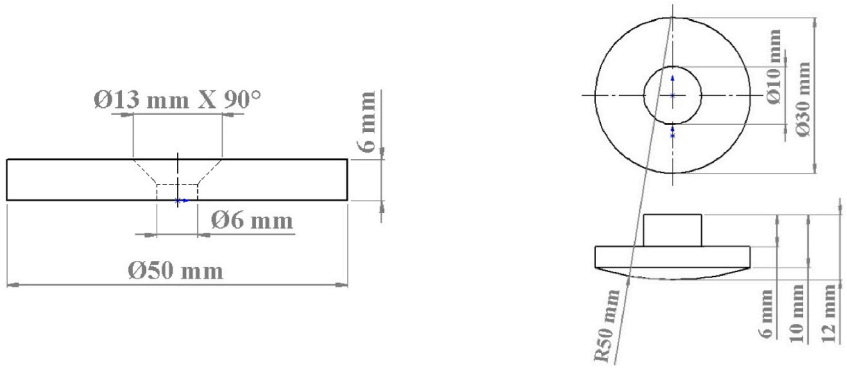

Fig. 5. Sketch **(a)** Disc sample **(b)** Pin sample.

Table 1
Properties of test specimens.

	Case-1	Case-2	Case-3
ID	Standard railway carbon steel	LC self-lubricating overlay	LC stainless steel overlay
pin	UIC60 900A rail steel, 0.6..0.8C, R_m = 880..1030 MPa, $A_5 \geq 10\%$. EN13674-1. Hardness 24 HRC (measured), ISO 21290 average roughness Ra ≈0.25 μm		
Disc material	R7 wheel steel UIC standard 812–3 (ER7 EN13262), C ≤ 0.52, R_m = 820..940 MPa, A≥14%.	LC overlay with Ni-based powder alloy containing 8% manganese sulphide (MnS) [31], disc substrate steel EN S235JR.	LC overlay with martensitic stainless steel powder alloy Rockit 401, Fe-0.15C–18Cr-0.5Mo-2.5N-<3 other (Höganäs AB) [32], disc substrate steel EN S235JR.
Disc surface roughness Ra (μm)	0.2	0.2	0.5
Disc hardness (HRC)	30	41[a]	51

[a] Hardness is biased with MnS-addition – the indenter penetration is lubricated.

inlet and outlet and the whole system was set to run for 10 min without any contact between the pin and the disc. The tests started when the concentration at the outlet became zero. To further ensure zero particles, only one test was run per day. The temperature variation was 20 ± 1 °C, and the relative humidity was 33 ± 1%.

3. Results

At first, friction and wear results are presented and followed by particle emission parameters.

3.1. Friction and wear

The average Coefficient of Friction (COF) of all repetitions for each case is presented against the sliding distance in Fig. 6 (a). Which depicts the steadiness of values. COF is also presented as a box and whisker plot for the sliding distance in Fig. 6 (b). For Case-1, with the standard railway carbon steels, and Case-3, with the LC test disc with stainless steel overlay, the COF follows the expected level of 0.44–0.52 with very narrow scattering around the mean value. However, for Case-2, for the test disc with the self-lubricating LC overlay, the COF has a mean value of about 0.22 but a larger scatter with a principal lower quartile of 0.15 and upper quartile of 0.35.

Fig. 7 Shows disc and pin mass loss, specific wear rate, and the total number concentration ranging from 6 nm to 10 μm and from 6 nm to 100 nm. For Case-1, standard railway steels, both pin and disc mass loss are relatively high for both pin and disc. The disc mass loss for Case-2 and Case-3, with LC self-lubricating respective LC stainless steel overlay, are very similar, whereas pin mass loss for Case-3 is more than as of Case-2 but like Case-1. This trend is also illustrated by the specific wear rate for discs and pins. For Case-3, the material composition of LC stainless steel overlay has a few times lower thermal diffusivity than

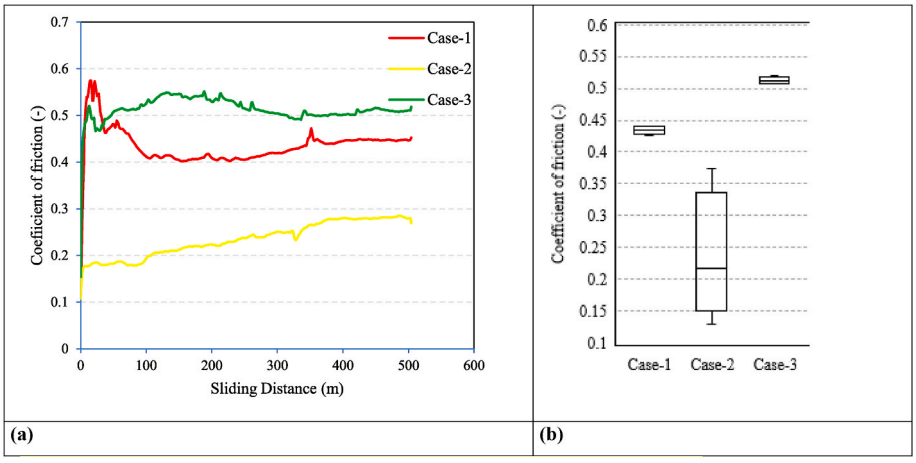

Fig. 6. (a) Coefficient of friction against total sliding distance **(b)** Coefficient of friction.

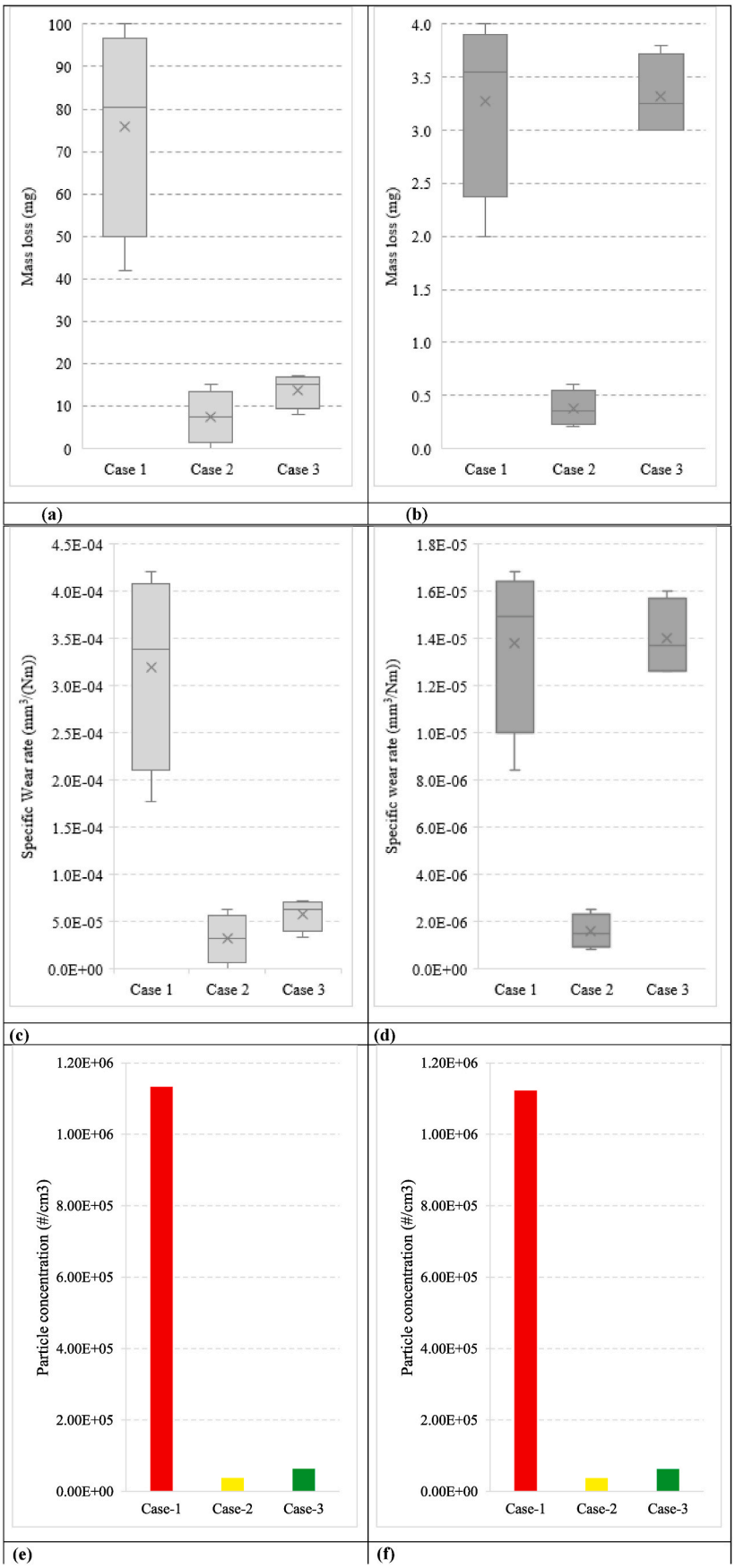

Fig. 7. (a) Disc mass loss **(b)** pin mass loss **(c)** disc specific wear rate **(d)** pin specific wear rate **(e)** total number concentration for 6 nm to 10 μm **(f)** total number concentration for 6 nm–100 nm.

carbon steel, and it likely increases the contact temperature. The COF here is slightly higher than Case-1 with standard railway carbon steels. For Case-2, the LC self-lubricating overlay has a material composition that, without MnS, should also have a thermal diffusion coefficient a few times lower than for Case-1 with standard railway carbon steels. However, the presence of 8% MnS-solid lubricant drops the COF to 0.22-level, which for sure drops the contact temperature. The total particle concentration for particle sizes 6 nm to 10 μm and 6 nm–100 nm are shown. The almost similarity of the plots shows that the particles emitted were almost in size range of 6 nm–100 nm.

Fig. 8 Shows the appearance of the pin and the disc worn surfaces. The appearance of the worn surface for Case-1 and Case-3 shows evidence of adhesive sliding wear with sliding wear marks with transferred worn material in the form of wear flakes. The appearance is similar, with a somewhat less severe appearance for LC stainless steel overlay in Case-3. However, for Case-2, the appearance is very different compared to the other two cases. Both the pin and the disc worn surfaces are very even and smooth. On the pin-worn surface, there is evidence of sliding wear marks but no wear-transferred material in the form of flakes. On the disc-worn surface, the wear track is narrower and smooth and shows sliding wear marks with much smaller and much less frequent occurring flakes. This description suggests, indeed, the presence of lubrication means - in this case, it was solid film lubrication with MnS.

3.2. Particle emission parameters

Particle emission parameters presented are total particle number, Fig. 9, and normalised particle size distribution, Fig. 10. Fig. 9 shows the particle numbers over the sliding distance measured via DEKATI ELPI+. The difference in the curve appearance is noticeable between Case-1 on one side and Case-2 and Case-3 on the other. After about 500 m in the sliding distance, all three curves appear to stabilise at 10^2 particles/cm^3, but the way to it is very different. For Case-1, the standard carbon railway steel, the particle number starts at 104 particles/cm^3 and quite linearly decreases to 10^2 particles/cm^3 after about 350 m. For Case-2, the LC self-lubricating disc, the particle number is always unchanged and keeps the particle number level at 10^2 particles/cm^3. For Case-3, the LC stainless steel disc, the particle number starts slightly below 10^3 particles/cm^3 but reaches the particle number level of 10^2 particles/cm^3 after about 100 m.

Fig. 10 shows the fraction of size distribution graph for all three cases. In all three cases, the emitted particles are in the ultra-fine range

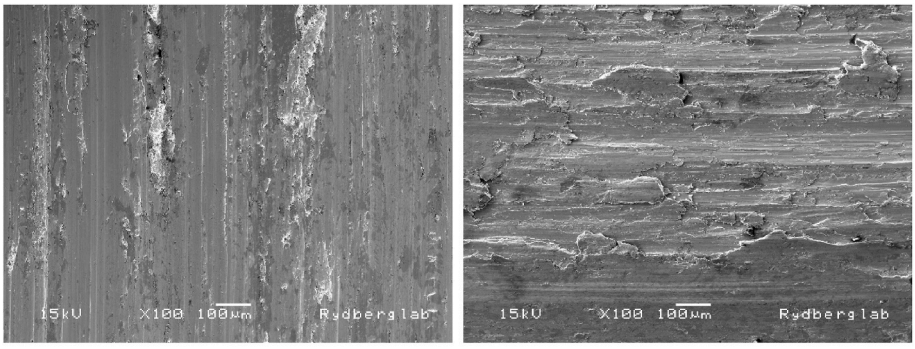

Case-1 – standards railway carbon steels

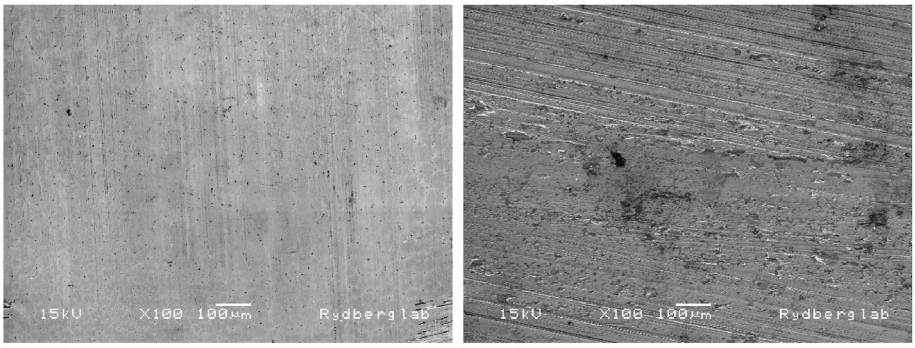

Case-2 – self-lubricating LC overlay.

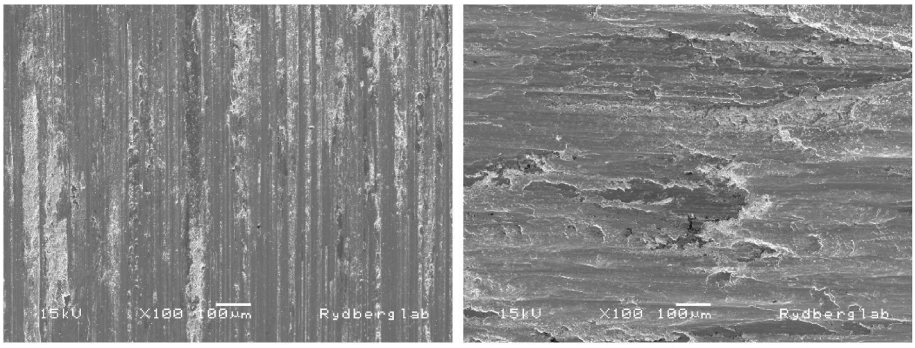

Case-3 – stainless steel LC overlay.

Fig. 8. Pin (left) and disc (right) worn contact area appearance.

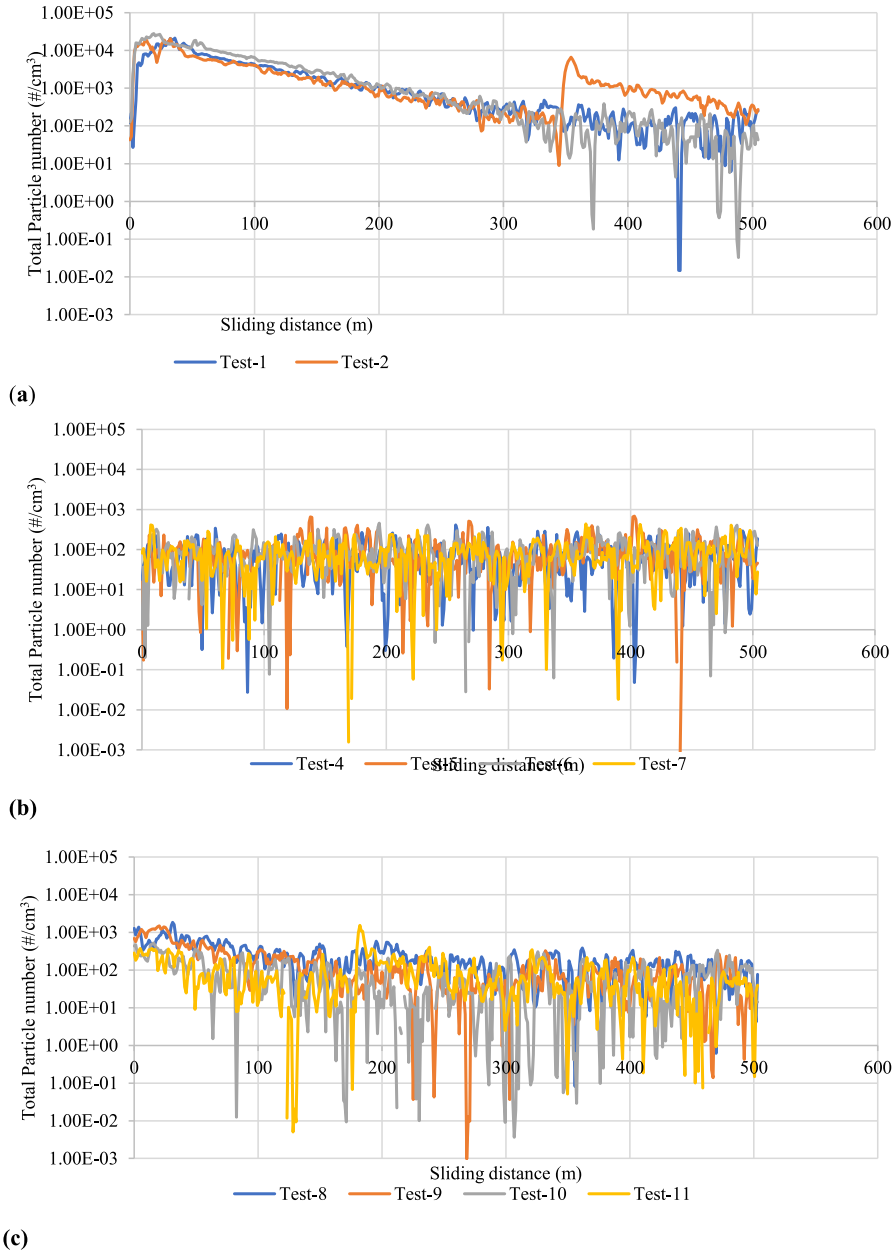

Fig. 9. Total particle number **(a)** Case-1 **(b)** Case-2 **(c)** Case-3.

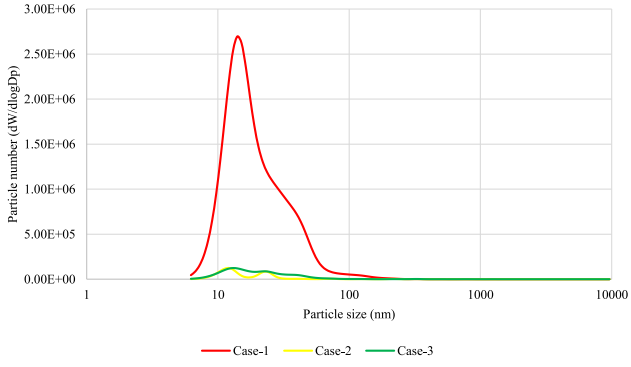

Fig. 10. Normalised particle size distribution.

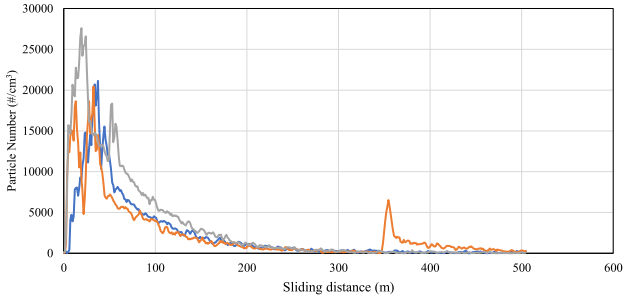

(a)

Fig. 11. Ultrafine particles for Case-1.

(6 nm–0.1 μm).

Fig. 11 presents the ultra-fine particle size range for Case-1 plotted against sliding distance which shows identical results for particle sizes ranging from 6 nm to 10 μm in Fig. 7(a) for Case-1. This is due to the reason that almost all the particles emitted were in the ultra-fine range. This plot is presented to illustrate it more precisely. The sharp peak at the start of the test shows that the particle number increase with an increase in sliding distance over time.

4. Discussion

In this study, dry wheel-rail contact was simulated on a dedicated pin-on-disc tribometer to study the influence of laser cladding on generated airborne particles. The generated airborne particles agree with the friction and wear rates and are supported by the SEM analysis. This type of study is difficult to perform in the field test due to the presence of pre-existing particles in the tunnels, whereas such background noise can be reduced easily in the lab by controlling the environmental conditions.

The results of the COF for all the cases are well within the acceptable limits for rail-wheel contact. From Fig. 6 (a) COF is relatively stable throughout the whole sliding distance for Case-1 and Case-3. Case-2 increases slightly over the sliding distance with a maximum value of 0.28 and an average value of 0.23 from all repetitions. This agrees with the acceptable values for such contact. Since the acceleration and braking usually require a COF of about 0.2. This value is most important in this type of contact for safety and performance reasons. An inadequate value can cause poor adhesin during braking, lead to extended stopping distance, and affect traction [33]. For Case-3, this value is averaged at 0.51, which is quite like the range reported in another research [34]. It is also suggested that values above 0.4 increase the chance of surface fatigue of wheels and rails [33]. Therefore, in terms of COF values, Case-2 yielded better results.

Firstly, from Fig. 9 (a), it can be confirmed that dry wheel-rail contact emits airborne particles, as reported in previous studies [9,35,36]. These particles were found mainly in the ultra-fine range (Fig. 10), which corresponds to a previous study [9]. In Ref. [9] it was found that the particle size generation mode varies with sliding velocity. More fine and ultrafine particles were observed when the sliding velocity was increased. In particular [9], showed that 90% of the generated particles had an aerodynamic diameter of less the 0.1 μm with a sliding velocity of 1.2 m/s, which agrees with the present study. An increased nanoparticle emission with an increase in train velocity under dry conditions is confirmed by another study [35] performed on the twin-disc rig, which simulated rolling/sliding and pure sliding. Also, in Ref. [36] on a similar test set-up as [35], the generated nanoparticles were higher than micro-particles when higher train velocities were simulated. This can be attributed to the results of [9] in which sliding velocity in a dry sliding wheel-rail contact is the crucial factor affecting the wear rate and could explain increased particle emission. Moreover, it can be seen from Fig. 9 (a) that the particle generation peaks at the test's start and then continues to settle down with time, covering almost 200 m of sliding distance. This could be due to the running-in period. Since most of the measured particles are in the sub-100 nm range and the particle concentration for the LC discs is 200–400 no/cm^3 for this size range, the results here are close to the sensitivity limit of the instrument. To distinguish the difference in particle concentration for the LC test specimens, an instrument with a lower sensitivity limit needs to be used in further studies.

The used contact condition is representative of a train running in a narrow curve, as from Ref. [8] in which the whole contact zone is sliding. In such a contact, a high contact temperature generates smaller wear fragments under a severe wear regime. This is also in line with a study by Olofsson and Olander [37] where it was demonstrated that the mild wear conditions representative of a train running on a straight track generates very few airborne wear fragments and a transfer to more severe conditions are needed for a more significant number of smaller size measurable airborne wear particles. From Fig. 10, most generated particles were in the ultrafine size range. Previous studies have shown that the generation of airborne particles in the ultrafine range is closely related to the contact temperature [38]. Ultrafine airborne particles are claimed to result from a thermal rather than a chemical process [39]. Oxidative wear was previously reported [9] as the likely mechanism for generating these particles. This type of wear is closely related to the ability of wear material to undergo oxidation and oxygen availability [40]. Oxidative wear is mainly a sliding wear mechanism and does not occur under lubricated conditions. Since it is a chemical process, it is more common in metals than other materials. However, in the present study, the SEM analysis of the worn pin and disc surfaces does not show any signs of oxide layers; instead, it shows evidence of adhesive wear for Case-1 and Case-3. The transfer worn material also indicates that sliding adhesive wear is the likely mechanism. This could be because the required temperature might not have been achieved to initiate the oxidative wear. For Case-2, the contact surfaces are smooth due to MnS, which acts as a solid lubricant. As discussed above, contact temperature plays a vital role in predicting the generation mechanism of airborne particles. In the present study, this contact temperature was not measured. It is recommended for future studies to measure this contact temperature by using more advanced techniques rather than thermocouples that can provide only the bulk temperature.

The reduction of particle emissions for Case-2 and Case-3, as shown in Fig. 9(b) and (c), is likely from the reduced wear rate. The specific wear rate is presented in Fig. 7. Different friction modifiers [25]and water lubricants [35] reduced emissions from the rail-wheel contact. In Ref. [35], it is that reported a negligible generation of microparticles occurred under wet conditions and suggested that water vapour might significantly influence the number of nanoparticles which agrees with [25] that the use of water-based lubricants in the wheel-rail contact can generate ultrafine particles.

If we scale up to the entire train wheel-rail contact, the particles generated will become huge in numbers in the case of traditional material contact. Laser cladding can be applied successfully to reduce the ultrafine particle emission from rail-wheel contact.

5. Conclusions

Using a pin-on-disc tribometer, the present study evaluated friction, wear, and airborne particle emissions for rail-wheel contact simulated in a lab environment. Test pins from standard UIC60 900A rail carbon steels were in contact with three types of test discs, standard R7 wheel carbon steel and structural steel test discs laser cladding overlayed with martensitic stainless steel and Ni-based-8% MnS self-lubricating alloy. The following conclusions are met.

- The coefficient of friction is 0.43 for as standard railway carbon steels, 0.51 when the test discs were laser-cladded with martensitic stainless steel and about halved, 0.23 when the test discs were laser-cladded with Ni-based-8% MnS self-lubricating alloy.
- The specific wear rate for the laser-cladded test discs is 10^{-5} mm^3/(Nm), about one ten power lower than for R7 wheel carbon steel.
- Test pins which were in contact with test discs laser-cladded with Ni-based-8% MnS self-lubricating alloy have a specific wear rate shows specific wear rate at a level of 10^{-5} mm^3/(Nm), about one ten power lower than for the other two discs.
- Airborne particle emission for the tests when discs are laser-cladded with Ni-based-8% MnS self-lubricating alloy is on a constant level of 200 particles/cm^3, for the disc's laser-cladded with martensitic steels starts at 300 and reaches 200 particles/cm^3 after a running-in of 200 m, and for the R7 wheel, carbon steel disc starts at 400 and reaches 200 particles/cm^3 after a running -in of 350 m.
- The use of laser-cladded overlay reduced the number of airborne wear particles in the sub-100 nm range by more than a factor of 10.

Declaration of competing interest

The authors declare the following financial interests/personal relationships which may be considered as potential competing interests: Ulf Olofsson reports financial support was provided by Horizon 2020 Research and Innovation. Senad Dizdar has patent #WO2018138247 pending to Senad Dizdar.

Data availability

The data that has been used is confidential.

Acknowledgements

This research received funding from European Union's Horizon 2020 research and innovation programme under grant agreement No. 954377 (nPETS project). The authors acknowledge the valuable contributions of Mr Lucas Bard and Dr Minghui Tu from KTH regarding the experimental set-up of this study.

References

[1] L. Zhao, L. Shen, The impacts of rail transit on future urban land use development: a case study in Wuhan, China, Transport Pol. 81 (2019) 396–405, https://doi.org/10.1016/j.tranpol.2018.05.004.
[2] T. Moreno, V. Martins, C. Reche, M.C. Minguillón, E. de Miguel, X. Querol, Chapter 13 - air quality in subway systems, Non-Exhaust Emissions (2018) 289–321, https://doi.org/10.1016/B978-0-12-811770-5.00013-3.
[3] Y. Zhou, H. Wang, H. Bi, J. Wang, Experimental and numerical study of aerodynamic pressures on platform screen doors at the overtaking station of a high-speed subway, Build. Environ. 191 (2021), 107582, https://doi.org/10.1016/j.buildenv.2020.107582.
[4] T. Moreno, V. Martins, X. Querol, T. Jones, K. BéruBé, M.C. Minguillón, F. Amato, M. Capdevila, E. de Miguel, S. Centelles, W. Gibbons, A new look at inhalable metalliferous airborne particles on rail subway platforms, Sci. Total Environ. 505 (2015) 367–375, https://doi.org/10.1016/j.scitotenv.2014.10.013.
[5] K. Vanherle, S. Lopez-Aparicio, H. Grythe, A. Lükewille, A. Uterstaller, I. Mayeres, Transport Non-exhaust PM-Emissions. An Overview of Emission Estimates, Relevance, Trends and Policies, 2021, https://doi.org/10.13140/rg.2.2.25720.98562.
[6] M.H. Jung, H.R. Kim, Y.J. Park, D.S. Park, K.H. Chung, S.M. Oh, Genotoxic effects and oxidative stress induced by organic extracts of particulate matter (PM10) collected from a subway tunnel in Seoul, Korea, Mutat. Res. 749 (2012) 39–47, https://doi.org/10.1016/j.mrgentox.2012.08.002.
[7] R. Lewis, U. Olofsson, 2 - basic tribology of the wheel–rail contact, Wheel–Rail Interface Handbook (2009) 34–57, https://doi.org/10.1533/9781845696788.1.34.
[8] R. Lewis, U. Olofsson, Mapping rail wear regimes and transitions, Wear 257 (2004) 721–729, https://doi.org/10.1016/j.wear.2004.03.019.
[9] H. Liu, Y. Cha, U. Olofsson, L.T.I. Jonsson, P.G. Jönsson, Effect of the sliding velocity on the size and amount of airborne wear particles generated from dry sliding wheel–rail contacts, Tribol. Lett. 63 (2016) 1–13, https://doi.org/10.1007/s11249-016-0716-5.
[10] J. Sundh, U. Olofsson, L. Olander, A. Jansson, Wear rate testing in relation to airborne particles generated in a wheel-rail contact, Lubric. Sci. 21 (2009) 135–150, https://doi.org/10.1002/ls.80.
[11] W.J. Wang, J. Hu, J. Guo, Q.Y. Liu, M.H. Zhu, Effect of laser cladding on wear and damage behaviors of heavy-haul wheel/rail materials, Wear 311 (2014) 130–136, https://doi.org/10.1016/j.wear.2014.01.011.
[12] Z.K. Fu, H.H. Ding, W.J. Wang, Q.Y. Liu, J. Guo, M.H. Zhu, Investigation on microstructure and wear characteristic of laser cladding Fe-based alloy on wheel/rail materials, Wear 330–331 (2015) 592–599, https://doi.org/10.1016/j.wear.2015.02.053.
[13] S.R. Lewis, R. Lewis, D.I. Fletcher, Assessment of laser cladding as an option for repairing/enhancing rails, Wear 330–331 (2015) 581–591, https://doi.org/10.1016/j.wear.2015.02.027.
[14] P. Lu, S.R. Lewis, S. Fretwell-Smith, D. Engelberg, D.I. Fletcher, R. Lewis, Laser Cladding of Rail; the Effects of Depositing Material on Lower Rail Grades, 2019, pp. 438–439, https://doi.org/10.1016/j.wear.2019.203045.
[15] L. Hua, R. Zhou, Damage and fatigue life evaluation for laser cladding remanufactured wheel, Adv. Mater. Sci. Eng. 2022 (2022) 1–7, https://doi.org/10.1155/2022/2060564.
[16] R. Vilar, Laser cladding, J. Laser Appl. 11 (1999) 64–79, https://doi.org/10.2351/1.521888.
[17] T. Schopphoven, A. Gasser, G.E.H.L.A. Backes, Extreme high-speed laser material deposition, Laser-Technik-Journal 14 (2017) 45, https://doi.org/10.1002/latj.201770308.
[18] LDF Series - Mobile High Power Diode Laser (2022). Available online: www.laserline.com.
[19] In-situ laser cladding, Available online: https://hardwear.com.au. (Accessed 29 November 2022).
[20] U. Olofsson, Y. Lyu, A.H. Åström, J. Wahlström, S. Dizdar, A.P.G. Nogueira, S. Gialanella, Laser cladding treatment for refurbishing disc brake rotors: environmental and tribological analysis, Tribol. Lett. 69 (2021), https://doi.org/10.1007/s11249-021-01421-1.
[21] Y. Lyu, M. Leonardi, A. Mancini, J. Wahlström, U. Olofsson, Tribology and airborne particle emission of laser-cladded Fe-based coatings versus non-asbestos organic and low-metallic brake materials, Metals 11 (2021) 1703, https://doi.org/10.3390/met11111703.
[22] S. Dizdar, Y. Lyu, C. Lampa, U. Olofsson, Grey cast iron brake discs laser cladded with nickel-tungsten carbide—friction, wear and airborne wear particle emission, Atmosphere 11 (2020) 621, https://doi.org/10.3390/atmos11060621.
[23] Bench Testing of Industrial Fluid Lubrication and Wear Properties Used in Machinery Applications, ASTM International, West Conshohocken, PA, 2006.
[24] Handbook of Railway Vehicle Dynamics, CRC Press, 2019.
[25] S. Abbasi, U. Olofsson, Y. Zhu, U. Sellgren, Pin-on-disc study of the effects of railway friction modifiers on airborne wear particles from wheel–rail contacts, Tribol. Int. 60 (2013) 136–139, https://doi.org/10.1016/j.triboint.2012.11.013.
[26] Olofsson, U.; Olander, L.; Jansson, A. A Study of Airborne Wear Particles Generated From a Sliding Contact, DOI: https://doi.org/10.1115/1.3176990.
[27] S. Andersson, 4 - friction and wear simulation of the wheel–rail interface, Wheel–Rail Interface Handbook (2009) 93–124, https://doi.org/10.1533/9781845696788.1.94.
[28] A. Matthews, K. Holmberg, Measurement of mechanical properties of thin solid films II: friction and wear, in: W. Gissler, H.A. Jehn (Eds.), Advanced Techniques for Surface Engineering, Springer Netherlands, Dordrecht, 1992, pp. 295–312.
[29] ELPI+™ USER MANUAL Ver. 1.12.
[30] J.A. Greenwood, J.B.P. Williamson, Contact of nominally flat surfaces, Proc. Roy. Soc. Lond. A 295 (1966) 300–319, https://doi.org/10.1098/rspa.1966.0242.
[31] S. Dizdar (inventor), New Product and Use Thereof, Patent application, WO2018138247.
[32] Rockit 401, Data Sheet, Höganäs AB, 2022.
[33] U. Olofsson, 17 - adhesion and friction modification, Wheel–Rail Interface Handbook (2009) 510–527, https://doi.org/10.1533/9781845696788.1.510.
[34] M. Harmon, J.F. Santa, J.A. Jaramillo, A. Toro, A. Beagles, R. Lewis, Evaluation of the coefficient of friction of rail in the field and laboratory using several devices, Tribol. Mater. Surface Interfac. 14 (2020) 119, https://doi.org/10.1080/17515831.2020.1712111.
[35] H. Lee, The effect of water lubricant on reducing the generation of airborne wear particles from wheel–rail contacts under various train velocities, Tribol. Int. 150 (2020), 106393, https://doi.org/10.1016/j.triboint.2020.106393.
[36] H. Lee, H. Namgung, S. Kwon, Effect of train velocity on the amount of airborne wear particles generated from wheel–rail contacts, Wear 414–415 (2018) 296–302, https://doi.org/10.1016/j.wear.2018.08.023.
[37] U. Olofsson, L. Olander, On the identification of wear modes and transitions using airborne wear particles, Tribol. Int. 59 (2013) 104–113, https://doi.org/10.1016/j.triboint.2012.01.013.
[38] H. Namgung, J. Kim, S. Woo, S. Park, M. Kim, M. Kim, G. Bae, D. Park, S. Kwon, Generation of nanoparticles from friction between railway brake disks and pads, Environ. Sci. Technol. 50 (2016) 3453–3461, https://doi.org/10.1021/acs.est.5b06252.
[39] A.T. Zimmer, A.D. Maynard, Investigation of the aerosols produced by a high-speed, hand-held grinder using various substrates, Ann. Occup. Hyg. 46 (2002) 663–672, https://doi.org/10.1093/annhyg/mef089.
[40] R. Lewis, R.S. Dwyer-Joyce, U. Olofsson, J. Pombo, J. Ambrósio, M. Pereira, C. Ariaudo, N. Kuka, Mapping railway wheel material wear mechanisms and transitions, Proc. Inst. Mech. Eng. - Part F J. Rail Rapid Transit 224 (2010) 125–137, https://doi.org/10.1243/09544097JRRT328.